On the consequences of side chain flexibility and backbone conformation on hydration and proton dissociation in perfluorosulfonic acid membranes

Stephen J. Paddison*[a] and James A. Elliott[b]

Received 14th February 2006, Accepted 16th March 2006
First published as an Advance Article on the web 28th March 2006
DOI: 10.1039/b602188c

The flexibility of the side chain and effects of conformational changes in the backbone on hydration and proton transfer in the short-side-chain (SSC) perfluorosulfonic acid fuel cell membrane have been investigated through first principles based molecular modelling studies. Potential energy profiles determined at the B3LYP/6-31G(d,p) level in the two pendant side chain fragments: $CF_3CF(–O(CF_2)_2SO_3H)–(CF_2)_7–CF(–O(CF_2)_2SO_3H)CF_3$ indicate that the largest $CF_2–CF_2$ rotational barrier along the backbone is nearly 28.9 kJ mol^{-1} higher than the minimum energy staggered *trans* conformation. Furthermore, the calculations reveal that the stiffest portion of the side chain is near to its attachment site on the backbone, with CF–O and O–CF_2 barriers of 38.1 and 28.0 kJ mol^{-1}, respectively. The most flexible portion of the side chain is the carbon–sulfur bond, with a barrier of only 8.8 kJ mol^{-1}. Extensive searches for minimum energy structures (at the B3LYP/6-311G(d,p) level) of the same polymeric fragment with 4–7 explicit water molecules reveal that the perfluorocarbon backbone may adopt either an elongated geometry, with all carbons in a *trans* configuration, or a folded conformation as a result of the hydrogen bonding of the terminal sulfonic acids with the water. These electronic structure calculations show that the fragments displaying the latter 'kinked' backbone possessed stronger binding of the water to the sulfonic acid groups, and also undergo proton dissociation with fewer water molecules. The calculations point to the importance of the flexibility in both the backbone and side chains of PFSA membranes to effectively transport protons under low humidity conditions.

Introduction

The transfer and transport of protons feature importantly in the function and energy transformation in a number of different chemical and biological systems.[1,2] Hence, the mechanisms of proton conduction are extensively studied both experimentally and theoretically in a variety of materials and diverse media[3] including: (most importantly) water,[4–8] mixed aqueous solutions (*e.g.* aqueous CH_3OH[9]), crystals,[10] solids[11,12] (*e.g.* oxides,[13] phosphates,[14] sulfates[15]), trans-membrane proteins[16–18] (*e.g.* proton channels[19] and pumps[20]), carbon nanotubes,[21] and polymer electrolyte membranes (PEMs).[22–29] Despite differences in the molecular structure of these systems there are common features including: the formation of a continuous network of dynamical hydrogen bonds and the mobility of the excess protonic charge with the centre of symmetry of the hydrogen bond coordination. The present work seeks to elucidate molecular features of proton transfer in minimally hydrated perfluorosulfonic acid (PFSA) polymers for the purposes of providing some direction towards the development of improved and highly conductive PEMs for fuel cells.[30,31]

[a] *Department of Chemistry and Materials Science, University of Alabama in Huntsville, Huntsville, AL 35899, USA. E-mail: paddison@matsci.uah.edu*
[b] *Department of Materials Science and Metallurgy, University of Cambridge, Pembroke Street, Cambridge, UK CB2 3QZ. E-mail: jae1001@cam.ac.uk*

PFSA membranes remain the most commonly employed electrolyte and electrode separator in PEM fuel cells due to a considerable window of chemical stability and mechanical strength. Nafion® (DuPont) is presently considered the state-of-the-art membrane in PEM fuel cells. Although now widespread, its use has some serious limitations including a restrictive range of thermal stability, high manufacturing cost and, most importantly, the need for a significant level of hydration in order to achieve sufficient proton conductivity.[32] The properties and function of a considerable number of PEMs have recently been reviewed by several authors.[33–39] The water in these biphasic systems is dispersed in a principally amorphous fluorocarbon polymeric primary phase.[40,41] The acidic groups of the polymer are solvated facilitating mobility of the protons *via* structural diffusion[42,43] through the hydrogen-bonded network of water molecules and conjugate bases (*i.e.* sulfonates) and vehicular diffusion where there is coupling of protons and water as hydronium ions.[44] The presence of water is critical for the formation of hydrated protons (*i.e.* as Zundel, $H_5O_2^+$, or Eigen, $H_9O_4^+$, cations) and their mobility. The hydration requirement of conventional PEMs results in a problematically low operating temperature limited by the boiling point of water (*i.e.* $T \leq 100$ °C at 1 atm). Since the PEM fuel cell is deemed to possess the potential to lead to considerable energy savings and security within a 'hydrogen economy', along with improvements in air quality, a substantial effort is being mounted to design and synthesize

improved high performance materials (such as membranes, catalysts, *etc.*).[45] The development of PEMs that can simultaneously operate above 100 °C and under low humidity conditions (thus without requiring pressurization of the system) whilst exclusively transporting protons is widely regarded as an important research and development requirement for fuel cell technology.

The design of PEMs possessing improved proton conductivity has been pursued *via* several different approaches.[34,46] These include: (i) replacement of the water by liquids such as phosphoric acid with polybenzimidazole,[47,48] phosphonic acid,[49] and imidazole;[50,51] (ii) addition of inorganic particles[35] (*e.g.* silica, heteropolyacids) to enable proton conductivity along the inorganic surface and retention of the absorbed water at elevated temperatures; and (iii) synthesis of entirely new ionomers. Along with these novel strategies has been the modification of the chemistry of the backbone, side chains, and even the protogenic groups. One of the earliest indications that the length of the side chain had an impact on membrane properties was reported for a short-side-chain (SSC) PFSA (*i.e.* a PTFE backbone with $-OCF_2CF_2SO_3H$ side chains)[52–55] first synthesized by the Dow Chemical Company.[56] Although SAXS and SANS measurements[53–55] indicated a hydrated morphology similar to Nafion, the proton conductivity was determined to be significantly higher at low to intermediate water contents.[28,57,58] The performance of this membrane in a fuel cell was also much improved over Nafion with current densities nearly three times higher at a potential of 0.5 V.[59] Although this material did not see widespread application in fuel cells or even further characterization, recently this membrane has become the subject of attention once again due to the development of a much simpler synthesis route by Solexis.[60] In addition, other PFSA membranes have been developed with distinct (to Nafion) side chain chemistries and have shown similar improved proton conductivity.[61,62] The reasons for the improved conductance are not fully understood, certainly not on a molecular basis, and hence provide the provocation for the present theoretical investigation.

Recent reviews[31,63,64] of theoretical studies into the mechanisms of proton conduction in PEMs indicate that although a considerable effort has been undertaken,[65–102] much remains to be understood in terms of how molecular chemistry and hydrated morphology dictate fuel cell performance. Molecular modelling of acidic functional groups, polymeric fragments, proton diffusion, and dielectric properties of the confined water in several different PEMs has suggested that the critical ingredients of proton conduction include complexity, connectivity and cooperativity, and that furthermore, the underlying chemical and physical processes need to be examined across diverse length and time scales. The complexity of proton conduction encompasses dissociation of the proton from the acidic site, subsequent transfer of the proton to the aqueous medium, separation of the hydrated proton from the conjugate base (*e.g.* the sulfonate anion), and finally diffusion of the proton in the confined water within the polymeric matrix. The connectivity involves not only hydrogen bonding of the water to the protogenic groups but also greater length scales including connection of the water domains within the polymeric matrix. Cooperative effects include the amphotericity of the protogenic groups and also the flexibility of the side chains and/or backbone. High frequency ($\leq$30 GHz) dielectric spectroscopy[103,104] and modelling of the dielectric saturation[83,93] of the water in PEMs reveal that the dissociated sulfonic acid groups (*i.e.* $-SO_3^-$) subject the confined water to a strong electrostatic field that increases the spatial and orientational order of the water molecules that is realized as a lower water permittivity (*i.e.* a dielectric constant <80).

Ab initio electronic structure calculations of polymeric fragments with water[65–68,84] and quantum molecular dynamics studies on model PEM systems[10] have revealed that: (i) the dissociated state is adopted as a result of the excess positive charge being stabilized in the hydrogen bonding network of the water molecules, and the excess electron density (due to the breaking of the $-SO_3-H$ bond) sufficiently delocalized by the neighbouring chemical group (anchimeric assistance); (ii) the neighbouring chemical group to the sulfonic acid will also affect the preferred separation of the hydronium ion after completion of the first hydration shell; (iii) hydrogen bonding between the sulfonic acid groups is favoured and, even with minimal water in the membrane, there is likely to be a continuous network of water formed among the $-SO_3H$ groups; (iv) partial dissociation of the protons in a PEM will occur at water contents of less than 3 H_2Os/SO_3H; and (v) the Zundel ion ($H_5O_2^+$) features importantly in the transfer of protons in PEMs of minimal hydration, as it does in bulk water. This latter result is based on extensive AIMD simulations[10,31] of trifluoromethanesulfonic acid monohydrate solid (a model system for minimally hydrated perfluorosulfonic acid PEMs) where an important defect structure was elucidated that possessed the distinctive features of two delocalized protons: one "shared" between two sulfonate groups and the other shared between two water molecules (*i.e.* a Zundel ion). With a formation free energy of only 30 kJ mol^{-1}, this result suggests that a possible pathway to developing minimally hydrated PEMs with high proton conductivity might be through the mobility of the acidic functional groups.

In earlier studies,[105,106] we sought to understand: (i) primary hydration of the sulfonic acid groups; (ii) the hydrogen bonding network of the 'chemical' water molecules connecting neighbouring pendant side chains (*i.e.* those sequential on the same backbone chain); and (iii) the role of the side chain in facilitating proton dissociation in fragments of the SSC ionomers with varying degrees of side-chain separation. Here, we restrict our attention to the $CF_3CF(-O(CF_2)_2SO_3H)-(CF_2)_7-CF(-O(CF_2)_2SO_3H)CF_3$ oligomeric fragment and determine its flexibility through computation of the rotational barriers of the backbone and all bonds along the length of one of the side chains. In addition, we report on the effects of conformational changes in the perfluorinated backbone on hydration and proton transfer in the oligomeric fragment with the addition of 4–7 explicit water molecules.

Computational method

Ab initio self-consistent field (SCF) molecular orbital calculations were performed using the GAUSSIAN 03 suite of programs[107] on Linux/MPI Beowulf clusters consisting of Intel Itanium 2 1.3, 1.4, and 1.5 GHz dual and quad processor

nodes. Full optimizations were undertaken by conjugate gradient methods[108] without symmetry constraints using Hartree–Fock theory with the 6-31G(d,p) split valence basis set[109] from initial structures with the fluorocarbon backbone, side chains, and water molecules in particular configurations and orientations. The resulting equilibrium structures were then further refined using density functional theory with Becke's 3 parameter functional (B3LYP),[110–112] initially with the same 6-31G(d,p) basis set and finally with the slightly larger 6-311G(d,p).[113] The effects of diffuse functions on the minimum energy structures were assessed and only minor differences in the structural parameters accompanied with a systematic difference in the total electronic energy was observed. Potential energy profiles were computed in the polymeric fragment displaying the lowest energy at the B3LYP/6-31G(d,p) level by systematically rotating about each of the bonds along one of the side chains and the carbon–carbon bonds located at the center of the backbone. Only the dihedral angle of the bond was constrained, and optimization was performed over all other degrees of freedom in the molecular fragment. We remark, in passing, on the difficulty of obtaining a smooth potential energy surface, despite rotating about the bond by only 5° increments. This would seem to be due to the side chain being caught in slightly higher energy conformations that the optimization scheme failed to relax. When this occurred we subsequently relaxed the single constraint, and performed a full optimization followed by a partial optimization at the same constrained dihedral angle. Vibrational frequencies and zero point energies (ZPEs) were determined for all global minimum energy structures of the fragment with water molecules at the B3LYP/6-311G(d,p) level. Binding energies of the water molecules to the oligomeric fragment were calculated from both the uncorrected and ZPE corrected total electronic energies. Finally, the effect of basis set superposition error (BSSE) on the water binding energies was explored using the commonly employed counterpoise (CP) method of Boys and Bernardi.[114,115] Although BSSE corrections have been known to change the order of local minima from that predicted by uncorrected energies,[116–118] it was not anticipated that this would be the case for these fragments due to the strong binding of the water to the sulfonic acid groups. Nevertheless, binding energies were computed from CP-corrected geometric optimizations[119,120] for all hydrated fragments.

Results and discussion

A Side chain flexibility

In a previous investigation[105] we obtained minimum energy structures for fragments of the SSC PFSA polymer with three different separations of the pendant side chains: 5, 7, and 9 CF_2 groups. We selected the polymeric fragment with 7 difluoromethylene units along the backbone for the present investigation to assess the flexibility of the side chain and backbone; and the global minimum energy structure is displayed in Fig. 1. As pointed out earlier,[105] this structure is the lowest energy conformation determined from five different starting configurations, and shows the side chains well separated from one another and positioned on the same side of the backbone.

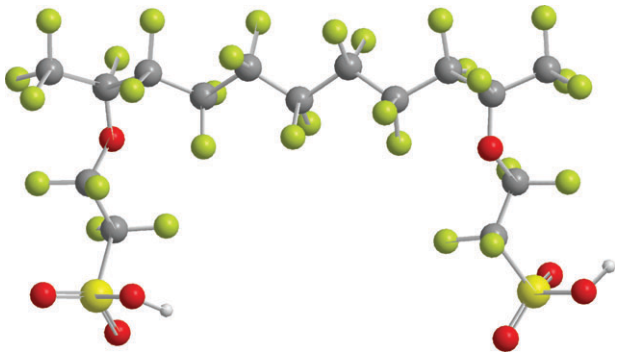

Fig. 1 Fully optimized (B3LYP/6-311G(d,p)) polymeric fragment. Grey spheres are carbon atoms, lime green spheres are fluorine atoms, red spheres are oxygen atoms, yellow spheres are sulfur atoms, and white spheres are hydrogen atoms.

Potential energy profiles were first determined at the point of attachment of the side chain to the perfluoro-backbone (*i.e.* the ether linkage) at the B3LYP/6-31G(d,p) level by constraining only the dihedral bond and then performing geometry optimizations at 5° increments in the dihedral incorporating the FC–O and O–CF_2 bonds, and are displayed in Fig. 2. It has generally been asserted that the ether linkages in the side chains provide flexibility and conformational freedom of the side chains. A prior first principles investigation by one of the authors[68] revealed that the rotational barrier of the outermost (from the PTFE backbone) ether linkage in the Nafion side chain was about 19.2 kJ mol^{-1}. Examination of the surfaces in Fig. 2, however, indicate that the barriers of the sole ether linkage of this SSC to the backbone are substantially greater with barriers of approximately 38.1 and 28.0 kJ mol^{-1} for the FC–O and O–CF_2 bonds, respectively. As the ether oxygen in both the long and short side PFSAs is attached to a similar tertiary carbon atom, the observed difference of nearly two-fold must be due to a rotation that places the side chain in close proximity to the PTFE backbone. The main barrier (at $\angle \approx -140°$) on the rotational potential surface of the FC–O bond is due to rotation that brings the F_2C–CF and O–CF_2 into an eclipsed *cis* conformation. The other much lower barrier (of approximately 15.8 kJ mol^{-1}) observed for this same bond at $\angle \approx 0°$, is a similar eclipsing of the O–CF_2 but with the terminal FC–CF_3 bond, and this indicates the penalty for interaction of the side chain with the backbone. The rotational barrier of 28.0 kJ mol^{-1} in the O–CF_2 bond is due to eclipsing the F_2C–CF_2 of the side chain with the F–C bond of the tertiary carbon where the side chain is attached to the backbone. We do point out that both of these surfaces are quite rough and at some points on the surface appear to be disjointed. This is possibly due to the inability of the minimization scheme[108] to locate a global minimum for the side chain (*i.e.* it becoming trapped in a high energy state as the dihedral angle is changed) and they are still rough despite a very substantial effort to smooth out the surface by performing numerous scans of the angle beginning from different points on the surface and also performing full optimizations on the partially optimized "high energy" structures. It is also

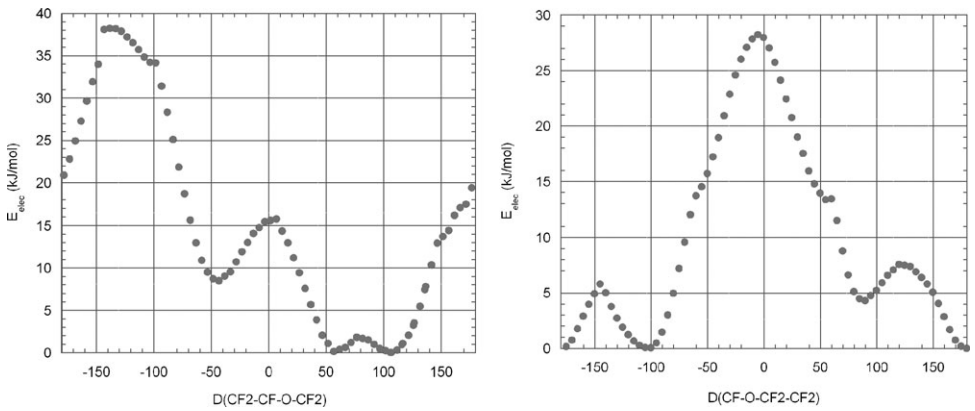

Fig. 2 Potential energy profiles for rotation about the FC–O (left) and O–CF_2 (right) bonds located at the attachment of the (right) side chain to the backbone in the oligomeric fragment (see Fig. 1) of the SSC PFSA membrane.

important to note that despite these significant barriers for the complete rotation of the side chain at its ether linkage to the backbone, there is a significant portion of the rotational surface where the energy of the fragment is less than 16 kJ mol^{-1} higher than the global minimum. This does suggest that there is considerable conformational freedom of the side chain at its attachment to the backbone despite a significant energetic penalty for complete rotation.

Potential energy surfaces were also computed for the carbon–carbon and carbon–sulfur bonds along the side chain and are plotted in Fig. 3. Although the magnitude of the rotational barrier (16.3 kJ mol^{-1}) for the F_2C–CF_2 bond is nearly twice that of the F_2C–S bond (8.8 kJ mol^{-1}) their profiles are quite similar, showing approximately a 3-fold degeneracy in the barriers and minima. These barriers occur when rotation of the chain results in eclipsing of either the C–F bonds with neighbouring C–F bonds or the C–F bonds with the S–O bonds. Both of these surfaces are somewhat smoother than those obtained for the bonds involving the ether oxygen (Fig. 2) and were much easier to compute. The energy barriers are also considerably lower for either the carbon–carbon or carbon–sulfur bonds than determined for the carbon–oxygen bonds. The energy penalty for rotation about the carbon–sulfur bond is significantly smaller than that previously reported by one of the authors[65] for trifluoromethane sulfonic acid where the barrier was calculated to be approximately 14.2 kJ mol^{-1}, but this is probably due to the fact that the calculations were performed at the MP2/6-31G* level.

Finally, a similar potential energy profile was determined for the sulfur–oxygen (protonated) bond at the B3LYP/6-31G(d,p) level and is shown in Fig. 4. There are two physically equivalent minima on this surface and two distinctly different maxima; the greatest at nearly 20.1 kJ mol^{-1} is due to a rotation that eclipses the O–H bond with the S–C bond. The lower barrier of about 2 kJ mol^{-1} is due to a rotation that points the acidic proton away from the side chain (a difference of 180° from the greater barrier). Previous molecular modelling of triflic acid[65] indicated that with the inclusion of electrostatic solvation (*i.e.* with a dielectric constant of 77.4 for the continuum) this lower barrier was reduced by nearly 4.2 kJ mol^{-1}. Clearly this suggests that the presence of water will affect the rotational barrier of this bond to the greatest extent (when compared to the other bonds along the length of the side chain) as the terminal portion of the side chain is the site of interaction with the water.

B. Backbone conformations

As a point of reference for later hydration studies with inclusion of explicit water molecules, we initially computed a

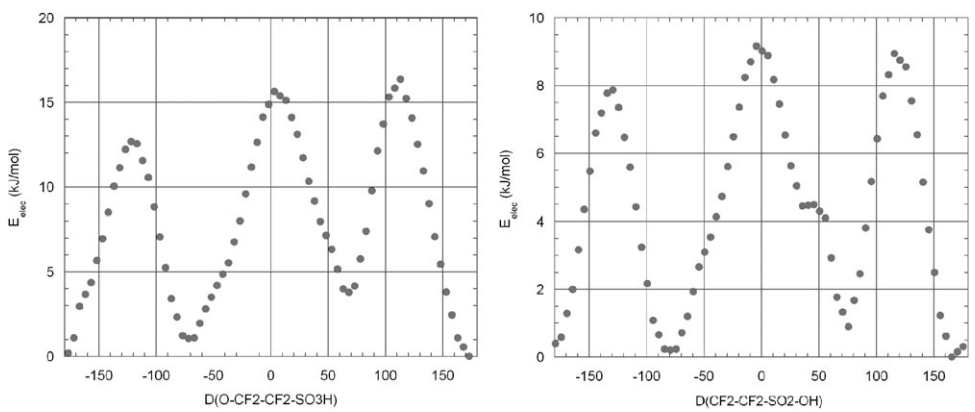

Fig. 3 Potential energy profiles for rotation about the F_2C–CF_2 (left) and F_2C–S (right) bonds along the (right) side chain in oligomeric fragment (see Fig. 1) of the SSC PFSA membrane.

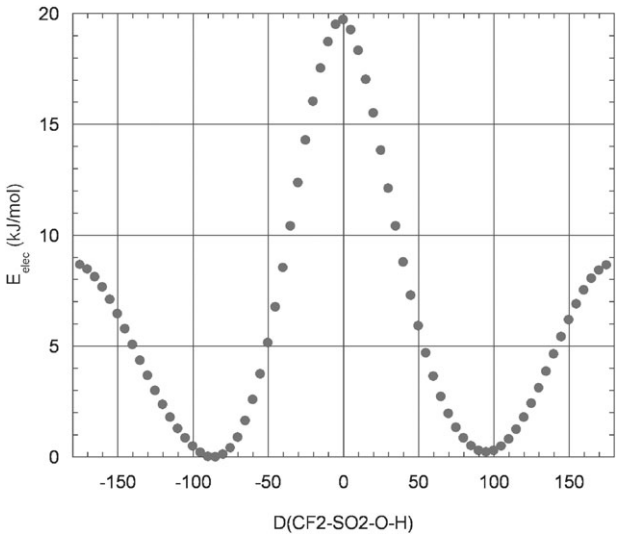

Fig. 4 Potential energy profile for rotation about the S–OH bond at the end of the side chain in oligomeric fragment of SSC PFSA membrane.

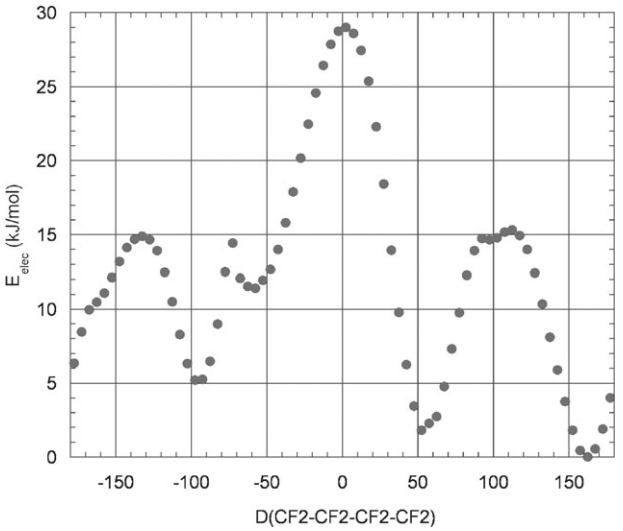

Fig. 5 Potential energy profile for rotation about the F_2C–CF_2 bond along the backbone in oligomeric fragment of SSC PFSA membrane.

similar potential energy profile (as those described above) for rotation of a central F_2C–CF_2 bond along the backbone. The calculated potential energy surface at the B3LYP/6-31G(d,p) level is shown in Fig. 5. The main barrier is a substantial 28.9 kJ mol^{-1} (at $\angle \approx 2.5^\circ$) higher than the staggered *trans* conformation and corresponds to a rotation that re-orientates the 1 and 4 carbons in the dihedral angle to a *cis* configuration. The other two significant maxima in the potential energy profile occur with barriers of approximately 15.9 kJ mol^{-1} and are due to rotation that eclipses the C–F bonds. Although there are three primary minima and maxima, in common with the profile determined for the C–C in bond side chain (Fig. 3), the energy of the *cis* barrier between *gauche* states in the backbone is significantly higher due to steric hindrance. Clearly, the backbone is significantly stiffer than the side chain.

Oligomeric fragments with 4 explicit water molecules. The total electronic energies, and (unscaled) zero point energies for the fully optimized (B3LYP/6-311G(d,p)) 'dry' fragment and two different conformations of the fragment with four explicit water molecules are given in Table 1. The data for the 'dry' fragment (see Fig. 1) are included for reference in the present work and for computing water binding energies. The minimum energy structures of these two 'hydrated' fragments are displayed in Fig. 6a and 6b and show two distinctly different backbone conformations: the first with an elongated backbone, and the second with a partially folded backbone. Binding energies of the water molecules to the fragment were computed from: (i) the uncorrected total electronic energies; (ii) zero point energy (ZPE) corrected total energies; and (iii) the counterpoise correction[114] of BSSE for re-optimized conformations, and are given in the fourth, fifth, and sixth columns of Table 1, respectively. Corresponding structural parameters for the minimum energy structure optimized under the CP scheme are given in Tables 2 (distances) and 3 (angles). These include the separation distance of the tertiary backbone carbons (*i.e.* those to which the side chains are attached), the separation of the sulfonic/ate sulfur atoms, the oxygen–acidic hydrogen distances (both when covalently bonded and after dissociation), the C–C–C–C dihedral angles along the backbone (from left to right), and all the dihedral angles along the length of the side chains (left, right).

Examination of the tabulated energies (Table 1) for 4*a* and 4*b* indicates that the magnitude of the binding energy per water molecule (in parentheses) decreases, on average, by 10.0 kJ mol^{-1} when ZPE is included and by a further 6.7 kJ mol^{-1} when BSSE is corrected in structures optimized under the CP scheme. It is also apparent that irrespective of the means of computing the binding energy, the water molecules bind more strongly in the structure with the partial folded backbone (*i.e.* 4*b*). The data in Table 2 indicate that the conformational change in the backbone has resulted in little change (less than 1 Å) in the distance between the tertiary carbons, but has brought the termini of the side chains (as measured by the sulfur–sulfur distance) considerably closer, by nearly 4 Å. This closer proximity of the two protogenic groups apparently gives stronger hydrogen bonding of the water to the oligomeric fragment. The 'kinking' of the backbone (Fig 6b) is due to an approximately 40° change in the first two C–C–C–C dihedral angles and to an even more dramatic decrease of nearly 80° in the third angle (see Table 3).

Comparison of the structural parameters of the two minimum energy fragments with the four explicit water molecules to the 'dry' fragment (Fig. 1) indicate that little conformational change has occurred in either side chain in fragment 4*a* (Fig. 6a). Only slight differences are observed in the C–C and C–S bonds of the right side chain, but these rotations have not taken the side chain from a minimum in the potential energy surfaces generated earlier (see Fig. 3), although the change in the dihedral angle of the C–S bond (from 74.5 to 163.0°) has surmounted a barrier of nearly 9 kJ mol^{-1} (third maximum in Fig 3 (right)). The side chains in the ionomeric fragment with the partially folded backbone (4*b*), however, have undergone

Table 1 Energetics of optimized $CF_3CF(–O(CF_2)_2SO_3H)–(CF_2)_7–CF(–O(CF_2)_2SO_3H)CF_3$ fragments[a]

$+n$ H_2O	E_{elec} [b]	E_{ZPE} [c]	ΔE [d] (kJ mol^{-1})	ΔE_{ZPE} [e] (kJ mol^{-1})	ΔE_{BSSE} [f] (kJ mol^{-1})	Δ_{a-b} [g] (kJ mol^{-1})
0	−4967.17008609	0.237984				
4*a*	−5273.05145130	0.324390	−240.6 (−60.2)[h]	−205.9 (−51.5)[h]	−178.2 (−44.3$_5$)[h]	37.2
4*b*	−5273.06643085	0.325406	−279.9 (−69.9)	−234.7 (−58.6)	−209.6 (−52.3)	
5*a*	−5349.55024136	0.363704	−375.3 (−74.9)	−325.1 (−64.8$_5$)	−273.2 (−54.8)	36.4
5*b*	−5349.56368352	0.367722	−410.5 (−82.0)	−348.1 (−69.5)	−309.6 (−61.9)	
6*a*	−5426.01195092	0.389560	−412.5 (−68.6)	−350.6 (−58.6)	−324.3 (−54.0)	46.9
6*b*	−5426.04019218	0.392711	−486.6 (−81.2)	−416.3 (−69.0)	−370.7 (−61.9)	
7*a*	−5502.48748578	0.413843	−486.2 (−69.5)	−416.3 (−59.4)	−370.3 (−52.7)	53.1
7*b*	−5502.51258810	0.418200	−552.3 (−79.1)	−470.7 (−67.4)	−423.4 (−60.7)	

[a] For structures optimized at the B3LYP/6-311G(d,p) level. [b] Total electronic energy in Hartrees. [c] Zero point energy (ZPE) in Hartrees. [d] Binding energy based on (uncorrected) total electronic energies. [e] Binding energy based on ZPE corrected E_{elec}. [f] Binding energy based on CP correction to BSSE of re-optimized structure. [g] CP corrected total energy difference between structure *a* and *b*. [h] Values in parentheses are per water molecule.

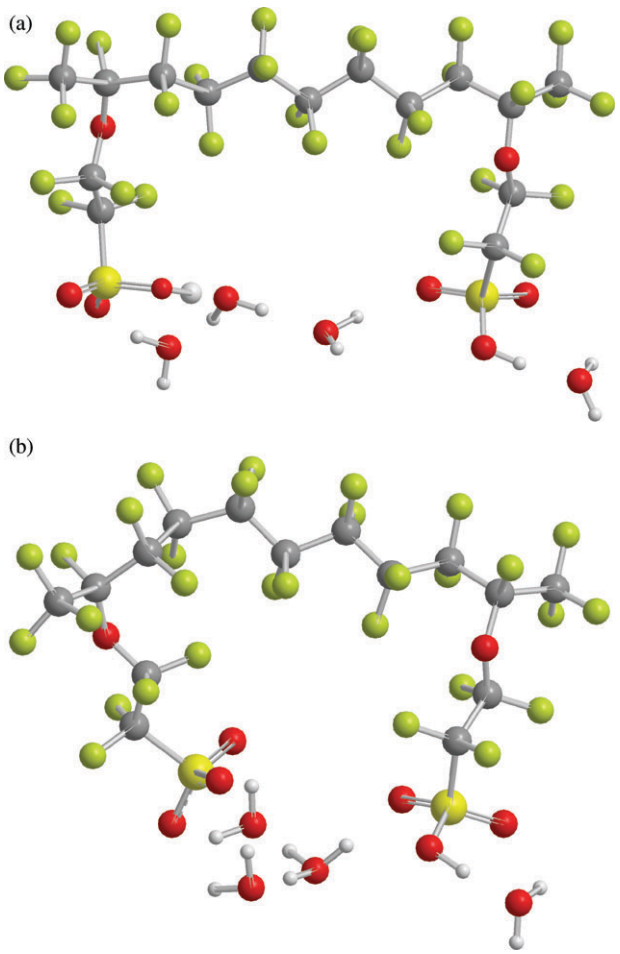

Fig. 6 Fully optimised (B3LYP/6-311G(d,p)) global minimum energy structures of the two side chain fragment with 4 explicit water molecules: (a) no dissociation of either acidic proton and PTFE backbone is elongated with the carbons in a *trans* conformation throughout; (b) one of the protons is dissociated and also separated from its conjugate base; the backbone has been folded with the sixth carbon from the left end in a nearly *cis* arrangement relative to the third carbon from the left end.

somewhat more significant conformational change, particularly the right side chain where the C–O bond has undergone rotation of more than 40°, corresponding to a point on the rotational potential surface of the 'dry' fragment that is

Table 2 Structural data[a] from optimized[b] $CF_3CF(–O(CF_2)_2SO_3H)–(CF_2)_7–CF(–O(CF_2)_2SO_3H)CF_3$ fragments

$+n$ H_2O	–CF···CF–	–S·····S–	–SO_2O···H	Fig. #
0	10.50	11.44	0.97, 0.97	1
4*a*	10.49	9.82	1.10, 1.01	6
4*b*	9.71	6.14	3.10, 1.03	6
5*a*	10.47	9.17	1.64, 1.01	7
5*b*	9.08	5.27	1.54, 1.53	7
6*a*	10.49	10.27	3.11, 1.01	8
6*b*	9.33	5.68	1.60, 1.54	8
7*a*	10.48	9.79	1.57, 1.32	9
7*b*	9.77	6.78	1.58, 1.52	9

[a] All atom distances in Å. [b] Optimized at the B3LYP/6-311G(d,p) level with CP correction to BSSE.

approximately 16.5 kJ mol^{-1} higher in energy. Clearly, even a few water molecules seem to allow the fragment to access energetic states *via* conformational changes in the backbone and/or side chains that are much higher than the global minimum energy configuration.

Of additional significance is the observation that while no transfer of either proton occurred in the fragment with the separated side chains (4*a*), dissociation and separation of one of the protons accompanies the slight folding of the backbone. The latter is particularly interesting as separation of a dissociated proton from single triflic acid molecules was not observed until the addition of six water molecules.[67,84] Finally, it is important to note that structure 4*b* is 37.2 kJ mol^{-1} lower in energy than structure 4*a* suggesting that the former is considerably more favourable than the latter.

Oligomeric fragments with 5 explicit water molecules. The B3LYP/6-311G(d,p) fully optimized structures of the two-side chain fragment with five water molecules exhibiting both the straight and a partially folded backbone are displayed in Fig. 7a and b, respectively, and the corresponding energetics and structural data in Tables 1–3. Comparison with the fragment with only four water molecules indicates that several new features have emerged. In the fragment with the elongated fully *trans* PTFE backbone (Fig. 7a), we see that the additional water molecule has brought about the dissociation of one of the protons and, as pointed out earlier,[105] an increase in the magnitude of the binding energy per water molecule of 10.5 kJ

Table 3 Structural data[a] from optimized[b] $CF_3CF(-O(CF_2)_2SO_3H)-(CF_2)_7-CF(-O(CF_2)_2SO_3H)CF_3$ fragments

$+n\ H_2O$	$\angle(CF_n–CF_2–CF_2–CF_m)$	$\angle(F_3C–FC–O–CF_2)$	$\angle(FC–O–CF_2–CF_2)$	$\angle(O–F_2C–CF_2–SO_3)$	$\angle(F_2C–F_2C–SO_2–OH)$	$\angle(F_2C–O_2S–O–H)$
0	170.7, 160.7, 161.7, 161.9, 161.7, 161.8, 161.0, 170.7	−39.9,−40.9	−173.5,−171.7	171.9,−166.0	−75.2,74.5	−88.9,−85.0
4*a*	167.8, 161.2, 157.1, 160.7, 159.7, 157.9, 160.6, 167.1	−43.8,−42.2	−172.3,−172.6	165.6,164.7	−80.9,163.0	−85.9,−94.9
4*b*	−164.7, −156.9, 79.9, 163.2, 161.8, 159.4, 161.6, 168.6	−82.5,−42.0	169.0,−170.3	159.9,174.1	−75.1,168.4	[c],−100.2
5*a*	167.4, 164.2, 152.2, 162.2, 159.2, 157.6, 160.9, 166.6	−45.3,−41.0	−172.0,−172.8	160.6,167.0	−85.7,163.3	[c],−94.0
5*b*	−170.3, −156.1, 84.3, 95.4, −178.6, 162.4, 161.2, 172.8	−47.3,−45.6	−162.8,−177.3	−176.1,163.8	−34.3,−86.1	[c],[c]
6*a*	169.6, 161.9, 157.7, 161.2, 160.7, 160.6, 160.6, 168.7	−41.8,−41.8	−175.0,−171.5	168.0,169.1	−85.7,172.3	[c],−99.6
6*b*	−162.4, −155.8, 69.2, 130.4, 172.0, 148.5, 166.8, 172.5	−37.0,−48.9	−169.5,−175.4	−172.6,163.3	−35.1,−91.2	[c],[c]
7*a*	169.1, 161.3, 161.0, 161.3, 164.0, 160.3, 163.8, 168.9	−41.2,−46.5	−171.7,−167.2	176.9,158.7	−62.7,166.7	[c],27.3
7*b*	−161.7, −169.0, 62.2, 154.9, 164.2, 161.4, 164.6, 167.6	−72.3,−47.3	154.5,−163.1	162.9,150.2	43.0,177.7	[c],[c]

[a] All angles in degrees (°). [b] Optimized at the B3LYP/6-311G(d,p) level with CP correction to BSSE. [c] Proton has dissociated and has been subsequently transferred to water molecules during optimization.

mol^{-1} (with CP correction to BSSE). However, the overall conformation of the fragment remains very similar to that of Fig. 6a with the distance between the tertiary carbons virtually unchanged and the termini of the side chains about 0.6 Å closer. The conformations of the side chains remain nearly unchanged with no more a 5° difference in any of the dihedral angles (see Table 3).

The changes in the oligomeric fragment are more extensive in the minimum energy conformation with the 'kinked' backbone. With five explicit water molecules both protons are transferred to the water molecules, which collectively now exist as a single hydrogen bonded water cluster. Further folding of the backbone has occurred with a nearly 70° decrease in the fourth C–C–C–C dihedral angle. The dissociation of the second proton has also been accompanied by an increase in the strength of the binding of the water molecules to the fragment. The binding energy per water molecule has increased by 9.6 kJ mol^{-1} when BSSE is corrected for with the CP scheme. Clearly, if the side chain termini are in close proximity to one another (less than 6 Å) and protons are transferred to the water, then a relatively strong constraint exists among the water molecules of the first hydration shell.

Comparing structural data from the two fragments possessing the folded backbones (*i.e.* 4*b* with 5*b* in Table 3), it is apparent that the addition of another water molecule has brought about a further folding of the backbone with a 67.8° rotation in the fourth dihedral angle into a *gauche* conformation. Both side chains in the latter fragment are oriented with similar dihedral angles at their attachment to the backbone, but at their termini substantial rotation of both C–S bonds has brought the two sulfonate groups significantly closer by nearly 0.9 Å. As before, the energy of the oligomeric fragment with the folded backbone is a significant 36.4 kJ mol^{-1} lower in energy than the fragment with the fully extended backbone emphasizing the importance of conformational changes in the PTFE component that facilitate closer proximity of the acidic groups with absorbed water.

Oligomeric fragments with 6 explicit water molecules. Computed binding energies and selected structural parameters for the oligomeric fragments with six water molecules are collected in Tables 1, 2 and 3. The B3LYP/6-311G(d,p) minimum energy structures with the backbone in an all *trans* configuration along with a partially folded geometry are displayed in Fig. 8a and b. Examination of these results continues to underscore the important differences in the hydration and proton transfer for different backbone conformations, as described earlier. Similar to what was observed in the fragments with 5 explicit water molecules, the fragment with the elongated backbone shows only a single dissociated proton despite the addition of another water molecule. This conformation shows a slight decrease in binding of the water to the fragment with a magnitude of only 54.0 kJ mol^{-1} per water molecule. Here, shown in Fig. 8a, the hydrated proton exists as a Zundel cation that is further separated ($r(O\cdots H) = 3.1$ Å) from the conjugate base with the backbone exhibiting essentially the same geometry as in the previously discussed conformations with fewer water molecules (*i.e.* Figs. 6a and 7a). Interestingly, the accommodation of the $H_5O_2^+$ ion has resulted in a slight increase in the separation of the side chains with the $S\cdots S$ distance nearly 10.3 Å. The fragment with the partially folded backbone is similar to that with the five water molecules (shown in Fig. 6b) with the third C–C–C–C dihedral angle nearly 15° smaller but the fourth 45° larger. We also observe the similarity with the two dissociated protons: where one is actually hydrogen bonded to both sulfonate groups, and is thereby responsible for the close proximity of the side chain termini; and the other Zundel-like in its connection to the two conjugate bases. The binding energy per molecule has remained unchanged from that computed with only five water molecules at 61.9 kJ mol^{-1}, and when compared to the fragment with the elongated backbone with the same number of water molecules, shows the significant stronger binding of the water to the protogenic groups. It is also worth noting that in comparing these two fragments with their distinctly

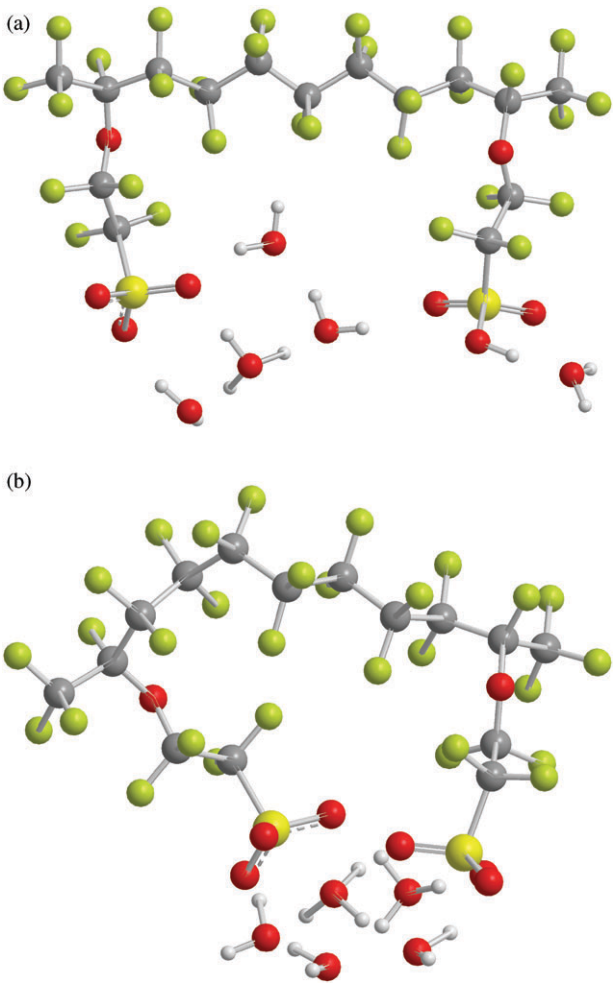

Fig. 7 Fully optimised (B3LYP/6-311G(d,p)) global minimum energy structures of the two side chain fragment with 5 explicit water molecules: (a) dissociation has occurred with only one of the sulfonic acid groups with hydrated proton exhibiting a Zundel-like structure and the PTFE backbone is elongated with the carbons in a *trans* conformation throughout; (b) both protons are dissociated with one as a hydronium ion hydrogen bonded to both sulfonates; the backbone is folded with both the sixth and seventh carbon atoms from the left in nearly *cis* arrangements.

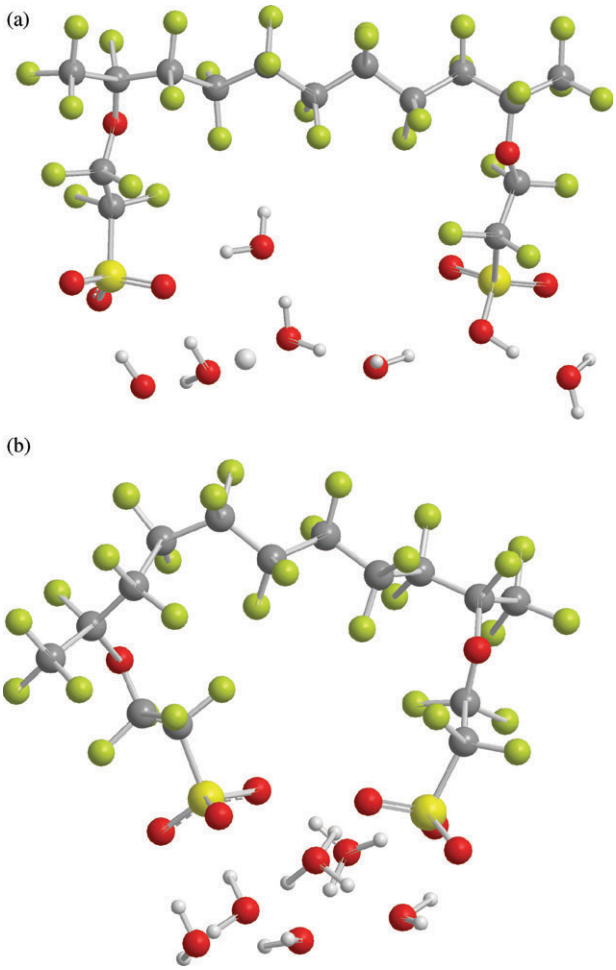

Fig. 8 Fully optimised (B3LYP/6-311G(d,p)) global minimum energy structures of the two side chain fragment with 6 explicit water molecules: (a) dissociation has occurred with only one of the sulfonic acid groups with the hydrated proton existing as a Zundel ion and the PTFE backbone is elongated with the carbons in a *trans* conformation throughout; (b) both protons are dissociated with one as a hydronium ion hydrogen bonded to both sulfonates; the backbone is folded with the sixth carbon from the left end in a nearly *cis* arrangement and seventh carbon showing significant departure from a *trans* arrangement.

different backbone conformations the energy difference is 46.9 kJ mol^{-1}, an increase of 10.5 kJ mol^{-1} over that observed in the fragments with five explicit water molecules.

In comparing the structural data for the fragments with 6 water molecules to their counterparts with only 5, only slight changes are observed in either the interatomic distances and the tabulated dihedral angles. The most significant difference is observed in the third and fourth dihderal angles (Table 3) where a decrease of 15.1° and an increase of 35.0° are observed, respectively.

Oligomeric fragments with 7 explicit water molecules. The fully optimized structures for the fragments with seven explicit water molecules, computed at the B3LYP/6-311G(d,p) level, are displayed in Fig. 9a and b. The corresponding energetics and structural data are again tabulated in Tables 1–3. The magnitude of the total binding energy decreases, similar to that observed with fewer water molecules, when compared across the methods according to the trend: $|\Delta E| > |\Delta E_{ZPE}| > |\Delta E_{BSSE}|$. It is worthy of note that the binding energy per water molecule for both backbone conformations has only changed very slightly (<2.1 kJ mol^{-1}) when compared to those calculated with only 6 explicit water molecules. However, in the fragment with all backbone carbons in a staggered *trans* configuration, the additional water has finally brought about the dissociation of the second proton, but as it is only around 1.3 Å from the sulfonate oxygen atom it is not completely transferred to the water molecule (*i.e.* the O···O distance is only 2.43 Å). We also note that the water molecules in this

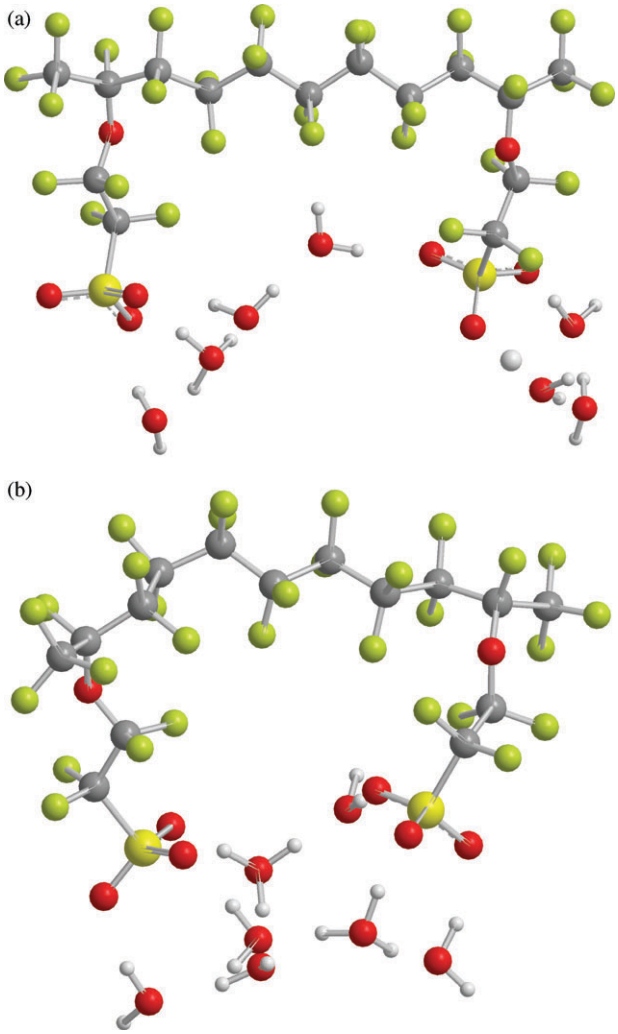

Fig. 9 Fully optimised (B3LYP/6-311G(d,p)) global minimum energy structures of the two side chain fragment with 7 explicit water molecules: (a) both protons are dissociated but exist in separate (*i.e.* not hydrogen bonded) water clusters; the PTFE backbone is elongated with the carbons in a *trans* conformation throughout; (b) both protons are dissociated with both in Zundel like structures bridging both sulfonates; the backbone is folded with the sixth carbon from the left end in a nearly *cis* arrangement.

fragment exist as two separated and protonated clusters consisting of 4 and 3 water molecules, respectively. This is, of course, in contrast to the fragment exhibiting the 'kinked' backbone, where all seven water molecules are hydrogen bonded in a single cluster that connects the two pendant sulfonate anions. With more than 53 kJ mol^{-1} difference in energy between these fragments, the latter with its continuous aqueous medium for proton transfer between (or at least in proximity to) the sulfonate groups is clearly the more favourable. We note that in the fragment of Fig. 9b, the sulfonate groups are slightly further apart than in any other fragment possessing a similar backbone geometry but with fewer water molecules; the sulfonate groups are now connected with Zundel-like ions.

Examination of the structural parameters of these oligomeric fragments reveals that the changes in backbone conformation upon folding (*i.e.* going from structure 7*a* to 7*b*) are qualitatively quite similar to those observed for fragments with six water molecules (*i.e.* 6*a* and 6*b*). However, some rotation of the first side chain in structure 7*b* has occurred as indicated by the more than 35° change in both the F_3C–FC–O–CF_2 and FC–O–CF_2–CF_2 dihedral angles. In addition, the C–S bonds of both side chains in this fragment with the folded backbone have rotated by 78.1 and 93.5°, respectively. Collectively, these conformational changes in the side chains have brought about an increase of 1.1 Å in the separation of the sulfonate groups.

Finally, it is worth noting that with the addition of the seventh water molecule, the magnitude of the water binding energy per water molecule has slightly decreased in both oligomeric fragments. This trend is expected to continue upon further addition of water molecules as the protonic charge is further solvated and the sulfonate groups screened.

Conclusions

We have studied the energetics (*i.e.* without inclusion of entropy) of the flexibility in both the backbone and side chain in the $CF_3CF(–O(CF_2)_2SO_3H)–(CF_2)_7–CF(–O(CF_2)_2–SO_3H)CF_3$ two side chain fragment of the SSC perfluorosulfonic acid membrane through a first principles based computation of rotational potential surfaces. Potential energy profiles determined at the B3LYP/6-31G(d,p) level indicate that the backbone is relatively stiff, with a maximum energy barrier of more than 29.0 kJ mol^{-1} between the staggered *trans* and planar *cis* conformations of the carbon atoms. Furthermore, the calculations revealed that the stiffest portion of the side chain is near its attachment to the backbone with the FC–O and O–CF_2 barriers of 38.1 and 28.0 kJ mol^{-1}, respectively. The most flexible portion of the side chain occurs at the point of attachment of the sulfonic acid group where the rotational barrier of the carbon–sulfur bond was determined to be only 8.8 kJ mol^{-1}.

Our electronic structure calculations of the same two side chain fragment of this perfluorosulfonic acid polymer indicates that the conformation of the PTFE backbone may have considerable effect on the hydration and transfer of protons to the aqueous environment. Specifically, it was found that when the backbone was partially folded and thereby allowed for the close proximity (less than 6.5 Å) of the sequential sulfonic acid groups, this resulted in stronger binding of the water to the protogenic groups. The electronic structure calculations also revealed that the oligomeric fragments exhibiting a 'kinked' backbone were more energetically favourable over those with the elongated backbone (*i.e.* a helically staggered *trans* configuration of backbone carbons). Finally, it was observed that the number of water molecules required to effect proton dissociation was reduced when the sulfonic acid groups were brought closer to each other through conformational change in the backbone. Thus our work has provided a benchmark set of results for which the effects of distinct and mixed protogenic groups, the consequences of differing side chain lengths, and local chemical composition may be examined.

Acknowledgements

The authors gratefully acknowledge financial support from the Engineering and Physical Sciences Research Council (EPSRC) of the UK, and SJP thanks the University of Alabama Huntsville for financial support in the purchase of one of the Beowolf clusters used in this work.

References

1 *Proton Conductors: Solids, membranes and gels—materials and devices*, ed. P. Colomban, Cambridge University Press, Cambridge, 1992.
2 K. D. Kreuer, *Chem. Mater.*, 1996, **8**, 610.
3 *Proton Conduction in Diverse Media*, a meeting organized by J. A. Elliott and S. J. Paddison, Fitzwilliam College, University of Cambridge, April 11–12, 2005, http://www.srcf.ucam.org/~jae1001/proton_meeting/.
4 M. Tuckerman, K. Laasonen, M. Sprik and M. Parrinello, *J. Chem. Phys.*, 1995, **103**, 150.
5 N. Agmon, *Chem. Phys. Lett.*, 1995, **244**, 456.
6 D. Marx, M. E. Tuckerman, J. Hutter and M. Parrinello, *Nature*, 1999, **397**, 601.
7 T. J. F. Day, U. W. Schmitt and G. A. Voth, *J. Am. Chem. Soc.*, 2000, **122**, 12027.
8 H. Lapid, N. Agmon, M. K. Petersen and G. A. Voth, *J. Chem. Phys.*, 2005, **122**, 014506.
9 J. A. Marrone and M. E. Tuckerman, *J. Chem. Phys.*, 2002, **117**, 4403.
10 M. Eikerling, S. J. Paddison, L. R. Pratt and T. A. Zawodzinski Jr, *Chem. Phys. Lett.*, 2003, **368**, 108.
11 R. C. T. Slade and M. J. Omana, *Solid State Ionics*, 1992, **58**, 195.
12 L. Rosso and M. E. Tuckerman, *Solid State Ionics*, 2003, **161**, 219.
13 K. D. Kreuer, *Annu. Rev. Mater. Res.*, 2003, **33**, 333.
14 T. Dippel, K. D. Kreuer, J. C. Lassègues and D. Rodriguez, *Solid State Ionics*, 1993, **61**, 41.
15 A. I. Baranov, L. A. Shuvalov and N. M. Schagina, *JETP Lett.*, 1982, **36**, 459.
16 T. E. DeCoursey, *Physiol. Rev.*, 2003, **83**, 475.
17 A. M. Smondyrev and G. A. Voth, *Biophys. J.*, 2002, **83**, 1987.
18 Y. J. Wu and G. A. Voth, *Biophys. J.*, 2003, **85**, 864.
19 R. Pomès and B. Roux, *Biophys. J.*, 2002, **82**, 2304.
20 T. E. DeCoursey and V. V. Cherny, *Isr. J. Chem.*, 1999, **39**, 409.
21 C. Dellago, M. M. Naor and G. Hummer, *Phys. Rev. Lett.*, 2003, **90**, 105902.
22 T. A. Zawodzinski, M. Neeman, L. O. Sillerud and S. Gottesfeld, *J. Phys. Chem.*, 1991, **95**, 6040.
23 T. A. Zawodzinski, T. E. Springer, J. Davey, R. Jestel, C. Lopez, J. Valerio and S. Gottesfeld, *J. Electrochem. Soc.*, 1993, **140**, 1981.
24 K. D. Kreuer, *Solid State Ionics*, 1997, **97**, 1.
25 C. A. Edmondson, P. E. Stallworth, M. E. Chapman, J. J. Fontanella, M. C. Wintersgill, S. H. Chung and S. G. Greenbaum, *Solid State Ionics*, 2000, **135**, 419.
26 H. Tang and P. N. Pintauro, *J. Appl. Polym. Sci.*, 2001, **79**, 49.
27 J. Kerres, A. Ullrich and M. Hein, *J. Polym. Sci., Part A: Polym. Chem.*, 2001, **39**, 2874.
28 S. K. Young and K. A. Mauritz, *J. Polym. Sci., Part B: Polym. Phys.*, 2002, **40**, 2237.
29 Y.-L. Ma, J. S. Wainright, M. H. Litt and R. F. Savinell, *J. Electrochem. Soc.*, 2004, **151**, A8.
30 K. D. Kreuer, *Solid State Ionics*, 2000, **136–137**, 149.
31 S. J. Paddison, *Annu. Rev. Mater. Res.*, 2003, **33**, 289.
32 K. D. Kreuer, *ChemPhysChem*, 2002, **3**, 771.
33 M. Doyle and G. Rajendran, in *Handbook of Fuel Cells—Fundamentals, Technology and Applications Volume 3—Fuel Cell Technology and Applications*, ed. W. Vielstich, A. Lamm and H. Gasteiger, J. Wiley and Sons, Chichester, UK, 2003.
34 K. D. Kreuer, in *Handbook of Fuel Cells—Fundamentals Technology and Applications, Volume 3—Fuel Cell Technology and Applications*, ed. W. Vielstich, A. Lamm and H. Gasteiger, J. Wiley and Sons, Chichester, UK, 2003.
35 G. Alberti and M. Casciola, *Annu. Rev. Mater. Res.*, 2003, **33**, 129.
36 M. F. H. Schuster and W. H. Meyer, *Annu. Rev. Mater. Res.*, 2003, **33**, 233.
37 J. Roziere and D. J. Jones, *Annu. Rev. Mater. Res.*, 2003, **33**, 503.
38 K. A. Mauritz and R. B. Moore, *Chem. Rev.*, 2004, **104**, 4535.
39 M. A. Hickner, H. Ghassemi, Y. S. Kim, B. R. Einsla and J. E. McGrath, *Chem. Rev.*, 2004, **104**, 4613.
40 G. Gebel and J. Lambard, *Macromolecules*, 1997, **30**, 7914.
41 G. Gebel, *Polymer*, 2000, **41**, 5829.
42 M. Eigen and L. De Maeyer, *Proc. R. Soc. London, Ser. A*, 1958, **247**, 505.
43 M. Eigen, *Angew. Chem.*, 1963, **75**, 489.
44 K. D. Kreuer, *J. Membr. Sci.*, 2001, **185**, 29.
45 B. C. H. Steele and A. Heinzel, *Nature*, 2001, **414**, 345.
46 J. A. Kerres, *J. Membr. Sci.*, 2001, **185**, 3.
47 J. S. Wainright, J. T. Wang, D. Weng, R. F. Savinell and M. H. Litt, *J. Electrochem. Soc.*, 1995, **142**, L121.
48 X. Glipa, B. Bonnet, B. Mula, D. J. Jones and J. Rozière, *J. Mater. Chem.*, 1999, **9**, 3045.
49 H. R. Allcock, M. A. Hofmann, C. M. Ambler, S. N. Lvov, X. Y. Y. Zhou, E. Chalkova and J. Weston, *J. Membr. Sci.*, 2002, **201**, 47.
50 K. D. Kreuer, A. Fuchs, M. Ise, M. Spaeth and J. Maier, *Electrochim. Acta*, 1998, **43**, 1281.
51 A. Bozkurt, W. H. Meyer and G. Wegner, *J. Power Sources*, 2003, **123**, 126.
52 M. R. Tant, K. P. Darst, K. D. Lee and C. W. Martin, in *Multiphase Polymers: Blends and Ionomers*, ed. L. A. Utracki and R. A. Weiss, ACS Proceedings Series 395, Washington, D. C., 1989, pp. 370–400.
53 R. B. Moore and C. R. Martin, *Macromolecules*, 1989, **22**, 3594.
54 J. Halim, F. N. Büchi, O. Hass, M. Stamm and G. G. Scherer, *Electrochim. Acta*, 1994, **39**, 1303.
55 G. Gebel and R. B. Moore, *Macromolecules*, 2000, **33**, 4850.
56 B. R. Ezzell, W. P. Carl and W. A. Mod, *Inventors*, The Dow Chemical Company, Assignee, 1982, US patent 4,358,412.
57 T. A. Zawodzinski, T. E. Springer, J. Davey, R. Jestel, C. Lopez, J. Valerio and S. Gottesfeld, *J. Electrochem. Soc.*, 1993, **140**, 1981.
58 C. A. Edmondson and J. J. Fontanella, *Solid State Ionics*, 2002, **152–153**, 355.
59 K. Prater, *J. Power Sources*, 1990, **29**, 239.
60 V. Arcella, A. Ghielmi and G. Tommasi, *Ann. N. Y. Acad. Sci.*, 2003, **984**, 226.
61 Z. Y. Yang and R. G. Rajendran, *Angew. Chem., Int. Ed.*, 2005, **44**, 564.
62 S. Hamrock, presented at *Advances in Materials for Proton Exchange Membrane Fuel Cell Systems 2005*, Pacific Grove, CA, February 20–23, 2005.
63 S. J. Paddison, in *Handbook of Fuel Cells – Fundamentals, Technology and Applications Volume 3—Fuel Cell Technology and Applications*, ed. W. Vielstich, A. Lamm and H. Gasteiger, J. Wiley and Sons, Chichester, UK, 2003.
64 K. D. Kreuer, S. J. Paddison, E. Spohr and M. Schuster, *Chem. Rev.*, 2004, **104**, 4637.
65 S. J. Paddison, L. R. Pratt, T. Zawodzinski and D. W. Reagor, *Fluid Phase Equilib.*, 1998, **150–151**, 235.
66 S. J. Paddison and T. A. Zawodzinski Jr, *Solid State Ionics*, 1998, **113–115**, 333.
67 S. J. Paddison, L. R. Pratt and T. A. Zawodzinski Jr, in *Proton Conducting Membrane Fuel Cells II, 98–27*, ed. S. Gottesfeld and T. F. Fuller, The Electrochemical Society Proceedings Series, Pennington, NJ, USA, 1999, pp. 99–105.
68 S. J. Paddison, L. R. Pratt and T. A. Zawodzinski Jr, *J. New Mater. Electrochem. Syst.*, 1999, **2**, 183.
69 S. J. Paddison, R. Paul and T. A. Zawodzinski Jr, in *Proton Conducting Membrane Fuel Cells II, 98–27*, ed. S. Gottesfeld and T. F. Fuller, The Electrochemical Society Proceedings Series, Pennington, NJ, USA, 1999, pp. 106–120.
70 J. A. Elliott, S. Hanna, A. M. S. Elliott and G. E. Cooley, *Phys. Chem. Chem. Phys.*, 1999, **1**, 4855.
71 S. J. Paddison, R. Paul and T. A. Zawodzinski Jr, *J. Electrochem. Soc.*, 2000, **147**, 617.
72 P. Johansson, J. Tegenfeldt and J. Lindgren, *Electrochim. Acta*, 2000, **45**, 3055.

73 J. A. Elliott, S. Hanna, A. M. S. Elliott and G. E. Cooley, *Macromolecules*, 2000, **33**, 4161.
74 A. Vishnyakov and A. V. Neimark, *J. Phys. Chem. B*, 2000, **104**, 4471.
75 A. Vishnyakov and A. V. Neimark, *J. Phys. Chem. B*, 2001, **105**, 7830.
76 M. Eikerling and A. A. Kornyshev, *J. Electroanal. Chem*., 2001, **502**, 1.
77 M. Eikerling, A. A. Kornyshev, A. M. Kuznetsov, J. Ulstrup and S. Walbran, *J. Phys. Chem. B*, 2001, **105**, 3646.
78 S. J. Paddison, L. R. Pratt and T. A. Zawodzinski Jr, *J. Phys. Chem. A*, 2001, **105**, 6266.
79 S. J. Paddison, R. Paul and T. A. Zawodzinski Jr, *J. Chem. Phys*., 2001, **115**, 7753.
80 S. J. Paddison, R. Paul and B. S. Pivovar Jr, in *Direct Methanol Fuel Cells, 01–04*, eds. S. Narayanan, S. Gottesfeld and T. A. Zawodzinski, The Electrochemical Society Proceedings Series, Pennington, NJ, USA, 2001, pp. 8–13.
81 S. J. Paddison, R. Paul, K. D. Kreuer and T. A. Zawodzinski Jr, in *Direct Methanol Fuel Cells, 01–04*, ed. S. Narayanan, S. Gottesfeld and T. A. Zawodzinski, The Electrochemical Society Proceedings Series, Pennington, New Jersey, 2001, pp. 29–33.
82 R. Paul and S. J. Paddison, in *Advances in Materials Theory and Modelling—Bridging Over Multiple-Length and Time Scales*, ed. V. Bulatov, L. Colombo, F. Cleri, L. J. Lewis and N. Mousseau, Materials Research Society, Warrendale, PA, USA, 2001.
83 R. Paul and S. J. Paddison, *J. Chem. Phys*., 2001, **115**, 7762.
84 S. J. Paddison, *J. New Mater. Electrochem. Syst*., 2001, **4**, 197.
85 E. Spohr, P. Commer and A. A. Kornyshev, *J. Phys. Chem. B*, 2002, **106**, 10560.
86 P. Commer, A. G. Cherstvy, E. Spohr and A. A. Kornyshev, *Fuel Cells*, 2002, **2**, 127.
87 P. G. Khalatur, S. K. Talitskikh and A. R. Khokhlov, *Macromol. Theory Simul*., 2002, **11**, 566.
88 M. Eikerling, S. J. Paddison and T. A. Zawodzinski Jr, *J. New Mater. Electrochem. Syst*., 2002, **5**, 15.
89 S. J. Paddison, R. Paul and K. D. Kreuer, *Phys. Chem. Chem. Phys*., 2002, **4**, 1151.
90 S. J. Paddison and R. Paul, *Phys. Chem. Chem. Phys*., 2002, **4**, 1158.
91 R. Paul and S. J. Paddison, *Phys. Rev. E*, 2003, **67**, 016108.
92 R. Paul and S. J. Paddison, *Solid State Ionics*, 2004, **168**, 245.
93 R. Paul and S. J. Paddison, *J. Phys. Chem. B*, 2004, **108**, 13231.
94 E. Spohr, *Mol. Simul*., 2004, **30**, 107.
95 Y. Yang and P. N. Pintauro, *Ind. Eng. Chem. Res*., 2004, **43**, 2957.
96 S. S. Jang, V. Molinero, T. Cagin and W. A. Goddard, *J. Phys. Chem. B*, 2004, **108**, 3149.
97 M. Iannuzzi and M. Parrinello, *Phys. Rev. Lett*., 2004, **93**, 025901.
98 M. K. Petersen, F. Wang, N. P. Blake, H. Metiu and G. A. Voth, *J. Phys. Chem. B*, 2005, **109**, 3727.
99 S. S. Jang, S.-T. Lin, T. Cagin, V. Molinero and W. A. Goddard, *J. Phys. Chem. B*, 2005, **109**, 10154.
100 S. Urata, J. Irisawa, A. Takada, W. Shinoda, S. Tsuzuki and M. Mikami, *J. Phys. Chem. B*, 2005, **109**, 4269.
101 N. P. Blake, M. K. Petersen, G. A. Voth and H. Metiu, *J. Phys. Chem. B*, 2005, **109**, 24244.
102 R. Paul and S. J. Paddison, *J. Chem. Phys*., 2005, **123**, 224704.
103 S. J. Paddison, D. W. Reagor and T. A. Zawodzinski, *J. Electroanal. Chem*., 1998, **459**, 91.
104 S. J. Paddison, G. Bender, K. D. Kreuer, N. Nicoloso and T. A. Zawodzinski Jr, *J. New Mater. Electrochem. Sys*., 2000, **3**, 291.
105 S. J. Paddison and J. A. Elliott, *J. Phys. Chem. A*, 2005, **109**, 7583.
106 S. J. Paddison and J. A. Elliott, *Solid State Ionics*, 2006, in press.
107 M. J. Frisch, G. W. Trucks, H. B. Schlegel, G. E. Scuseria, M. A. Robb, J. R. Cheeseman, J. A. Montgomery Jr, T. Vreven, K. N. Kudin, J. C. Burant, J. M. Millam, S. S. Iyengar, J. Tomasi, V. Barone, B. Mennucci, M. Cossi, G. Scalmani, N. Rega, G. A. Petersson, H. Nakatsuji, M. Hada, M. Ehara, K. Toyota, R. Fukuda, J. Hasegawa, M. Ishida, T. Nakajima, Y. Honda, O. Kitao, H. Nakai, M. Klene, X. Li, J. E. Knox, H. P. Hratchian, J. B. Cross, C. Adamo, J. Jaramillo, R. Gomperts, R. E. Stratmann, O. Yazyev, A. J. Austin, R. Cammi, C. Pomelli, J. W. Ochterski, P. Y. Ayala, K. Morokuma, G. A. Voth, P. Salvador, J. J. Dannenberg, V. G. Zakrzewski, S. Dapprich, A. D. Daniels, M. C. Strain, O. Farkas, D. K. Malick, A. D. Rabuck, K. Raghavachari, J. B. Foresman, J. V. Ortiz, Q. Cui, A. G. Baboul, S. Clifford, J. Cioslowski, B. B. Stefanov, G. Liu, A. Liashenko, P. Piskorz, I. Komaromi, R. L. Martin, D. J. Fox, T. Keith, M. A. Al-Laham, C. Y. Peng, A. Nanayakkara, M. Challacombe, P. M. W. Gill, B. Johnson, W. Chen, M. W. Wong, C. Gonzalez and J. A. Pople, *GAUSSIAN 03 (Revision C.02)*, Gaussian, Inc., Wallingford, CT, 2004.
108 H. B. Schlegel, *J. Comput. Chem*., 1982, **3**, 214.
109 P. C. Hariharan and J. A. Pople, *Theor. Chim. Acta*, 1973, **28**, 213.
110 A. D. Becke, *J. Chem. Phys*., 1993, **98**, 1372.
111 A. D. Becke, *J. Chem. Phys*., 1993, **98**, 5648.
112 C. T. Lee, W. T. Yang and R. G. Parr, *Phys. Rev. B*, 1998, **37**, 785.
113 A. D. McLean and G. S. Chandler, *J. Chem. Phys*., 1980, **72**, 5639.
114 S. F. Boys and F. Bernardi, *Mol. Phys*., 1970, **19**, 55.
115 D. J. Donaldson, *J. Phys. Chem. A*, 1999, **103**, 62.
116 N. Kobko and J. J. Dannenberg, *J. Phys. Chem. A*, 2001, **105**, 1944.
117 D. Tzeli, A. Mavridis and S. S. Xantheas, *Chem. Phys. Lett*., 2001, **340**, 538.
118 J. Garza, J. Z. Ramírez and R. Vargas, *J. Phys. Chem. A*, 2005, **109**, 643.
119 D. B. Chesnut, *J. Phys. Chem. A*, 2002, **106**, 6876.
120 P. Salvador, M. Duran and J. J. Dannenberg, *J. Phys. Chem. A*, 2002, **106**, 6883.